Transp Porous Med (2009) 80:281–304
DOI 10.1007/s11242-009-9359-4

# Matrix Heterogeneity Effects on Gas Transport and Adsorption in Coalbed and Shale Gas Reservoirs

**Ebrahim Fathi · I. Yücel Akkutlu**

Received: 28 May 2008 / Accepted: 9 February 2009 / Published online: 3 March 2009


**Abstract** In coalbeds and shales, gas transport and storage are important for accurate prediction of production rates and for the consideration of subsurface greenhouse gas sequestration. They involve coupled fluid phenomena in porous medium including viscous flow, diffusive transport, and adsorption. Standard approach to describe gas–matrix interactions is deterministic and neglects the effects of local spatial heterogeneities in porosity and material content of the matrix. In this study, adopting weak-noise and mean-field approximations and using a statistical approach in spectral domain, matrix heterogeneity effects are investigated in the presence of non-equilibrium adsorption with random partition coefficient. It is found that the local heterogeneities can generate non-trivial transport and kinetic effects which retard gas release from the matrix and influence the ultimate gas recovery adversely. Macro-transport shows $1/[1 + N_{Pe}/(1 + N_{Pe})]$ dependence on the Péclet number, and persists at the diffusive ultra-low permeability limit. Macro-kinetics is directly related to Thiele modulus by the following expression: $N_{Th}/(1 + 2N_{Pe})$. It leads to trapping of gas in the adsorbed phase during its release from the matrix, and to an adsorption threshold during the gas uptake by the matrix. Both effects are proportional to the initially available adsorbed gas amount and becomes more pronounced with the increasing variance of the porosity field. Consequently, a new upscaled deterministic gas mass balance is proposed for practical purposes. Numerical results are presented showing free and adsorbed gas distributions and fractional gas sorption curves for unipore coal matrix exhibiting Gaussian porosity distribution. This study is a unique approach for our further understanding of the coalbeds and gas shales, and it is important for the development of sound numerical gas production and sequestration models.

**Keywords** Heterogeneity · Upscaling · Gas adsorption kinetics · Macro-transport · Macro-kinetics

E. Fathi · I. Y. Akkutlu
Mewbourne College of Earth and Energy, University of Oklahoma, Norman, USA

I. Y. Akkutlu (✉)
School of Petroleum and Geological Engineering, Sarkeys Energy Center, University of Oklahoma, Room T-311, 100 East Boyd, Norman, OK 73079-1003, USA
e-mail: akkutlu@ou.edu

### List of Symbols

| | |
|---|---|
| $B_0$ | Absolute coal permeability ($cm^2$) |
| $C$ | Free gas concentration (mol/cc pore) |
| $C_\mu$ | Adsorbed gas concentration (mol/cc solid) |
| $C_{\mu s}$ | Maximum adsorbed gas concentration (mol/cc solid) |
| $D$ | Molecular diffusion coefficient ($cm^2/s$) |
| $\mathcal{D}$ | Apparent diffusion coefficient ($cm^2/s$) |
| $E$ | Adsorbate adsorbent interaction energy (J/mol) |
| $g$ | Average free gas concentration (mol/cc) |
| $K$ | Partition (distribution) coefficient (fraction) |
| $k_\mathrm{f}$ | Gas adsorption rate coefficient (1/s) |
| $k_\mathrm{r}$ | Gas desorption rate coefficient (1/s) |
| $k_{\mathrm{r}\infty}$ | Gas desorption rate constant at zero energy level (1/s) |
| $R$ | Universal gas constant ($\mathrm{J\,K^{-1}\,mol^{-1}}$) |
| $r$ | Pore half width (cm) |
| $t$ | Time coordinate (s) |
| $T$ | Temperature (K) |
| $x$ | Space coordinate (cm) |

### Greek Symbols

| | |
|---|---|
| $\alpha$ | Effective drift velocity (m/s) |
| $\phi$ | Porosity (fraction) |
| $\Phi$ | Solid-to-bulk volume ratio (fraction) |
| $\sigma_\mathrm{f}^2$ | Variance of porosity fluctuations |
| $\mu$ | Gas viscosity (kg/cm s) |
| $\lambda$ | Porosity correlation length (cm) |

## 1 Introduction

Production from coalbeds and shale gas reservoirs make up nearly 15% of the total annual natural gas supply in the United States. Many other countries currently investigate the potential of these unconventional resources. Australia, Canada, China, and India have commercial projects on coal gas production, while others identify new shale gas resources as they consider the incremental shale gas production in the existing reservoir. These natural gas resources are estimated to exceed 25,000 Tscf globally and, under the projected energy portfolio, they are predicted to play an important role on energy supply (Jenkins and Boyer 2008).

Despite their commercial importance, exploitation of these resources raises technological challenges. Gas well productivities are influenced primarily by low-permeable nature of the reservoir formation. Porosity and absolute permeability of the matrices are significantly less than those belong to the conventional gas reservoirs, taking values typically in the range of a millidarcy in the producing areas. In addition, due to large internal surface areas of the matrices, coalbeds and gas shale formations containing significant amounts of organic matter (e.g., Devonian shales) retain a large portion of natural gas at an adsorbed state. The latter is a physical mechanism which plays an important role during the estimation of gas-in-place and the future reservoir predictions (King 1990).

Tight nature of the matrices and their ability to retain the gas at an adsorbed state also make these environments important gas trapping and storage locations. Coalbeds are considered to be one of the targeted subsurface environments for the greenhouse gas sequestration. Although no large-scale projects currently exist, field tests are being performed for $CO_2$ injection and enhanced coalbed methane production, i.e., $CO_2$–ECBM. Gas shales are also likely to play a role in sequestration similar in magnitude to coals in near future (Nuttall 2005).

A vibrant and fast-growing literature exists related to various aspects of coals and gas shales, including operational (e.g., drilling, completion, and production) and technological challenges. The latter mainly involves difficulties in formation evaluation/characterization, in modeling gas–matrix-fracture phenomena, and in developing reliable reservoir simulators. In times, these studies directly point to an inability to accurately predict the ultimate gas recovery and to explain high variability in gas well productivity, which are common to nearly all coalbed and shale gas reservoirs. Recently, Weida et al. (2005) quantified such variability using cumulative gas production data of a set of wells drilled and completed in essentially the same way (open-hole) in a small area in a single coal seam. Experience with the conventional resources prescribes that the observed variability in production is due to changes in effective reservoir permeability: under initial equilibrium conditions, since the natural gas is likely to be homogeneously distributed in the microstructure of the matrices, these variations should be due to spatial and temporal changes in permeability. This point of view emphasizes the existence of a dense network of fractures with a dynamic permeability field which changes in time due to opening and closing of fractures as the places of dominant transport for gas production. It may, however, overlook the influence of finer scale heterogeneities intrinsic to the matrices surrounded by those fractures and it may neglect their roles on the initial distribution of gas, and on the production. Now, it is recognized that coals and shales are in fact complex composite materials consisting of a large group of minerals and organic matter exhibiting an intricate pore structure even within the length of a meter. Applying X-ray computerized tomography (CT) imaging, Karacan (2003) recently quantified spatial distribution of micro-lithotypes in coal samples in the order of 1 cm in diameter. Further, he argued that equilibrium and non-equilibrium dynamics of gas adsorption process needs to be investigated carefully to understand gas–solid interactions and transport phenomena in the matrices.

The purpose of this article is to consider local phenomena in a heterogeneous matrix using a theoretical approach. We therefore first develop the means to appropriately quantify the local matrix heterogeneities and then to up-scale (or homogenize) the gas flow, diffusive transport, and adsorption processes over the matrix body. Hence, our study here builds on the premise that the local gas behavior in the matrix is simultaneously controlled by the gas sorption rates, viscous and diffusive gas mass fluxes. Although the matrix exhibits local variations in the pore structure, we consider that these local variations are weak and that the porous medium still maintains a meaningful average porosity and a constant permeability values. We then investigate analytically and numerically the effects of porosity fluctuations, in particular, and the related material property variations on the mechanisms of transport and storage. For the investigation, initially, we locally describe mass conservation for a gas component (for which the matrix has a certain adsorption capacity, e.g., methane) in homogeneous media characterized by a time-independent porosity in space–time continuum. Next, the classical perturbation theory is employed to the governing equations where the structural and chemical variations are introduced in terms of fluctuating (random) porosity and partition coefficient, respectively. The analytical part of our study is concerned with the description and analysis of the theoretical problem using the mean and perturbed governing equations in the Laplace–Fourier domain. The mean equations are, in fact, upscaled governing equations,

which include cross-correlations between porosity and dependent variables, reflecting the influences of the introduced small-scale porosity fluctuations on the adsorbed and free gas concentrations and on the Fickian-type diffusivity. Obtaining explicit expressions for the latter quantities are the most critical part of any work based on perturbations and noise analysis and, here, they are examined using the perturbed governing equations in the spectral domain. Similar approaches have been considered by several authors; see, for example, textbooks by Forster (1977) and Gelhar (1993), or publications by J.H. Cushman's group (e.g., Hu et al. 1995 and, recently, by L'Heureux (2004). Second part of this study involves numerical analysis of the upscaled governing equations describing gas adsorption and transport behavior in heterogeneous coal matrix. For this purpose, gas release from a matrix is considered and presented as a onedimensional initial/boundary value problem. Results showing the influence of heterogeneities on gas release rates are demonstrated using fractional gas recovery curves and comparing with the homogeneous case.

## 2 Local Gas Behavior in the Matrix—Homogeneous Case

### 2.1 Kinetics of Gas Adsorption in Porous Media

Perhaps the earliest discussion on the existence of local conditions which require kinetics description of adsorption in coals and shales figures in King (1990), who suggested that the assumption of equilibrium adsorption may be appropriate only in reservoirs undergoing rapid desorption, such as in the vicinity of producing wells. In the latter case, an explicit algebraic equation, i.e., an equilibrium adsorption isotherm, describing a relationship between the adsorbed and free gas amounts is introduced:

$$C_\mu = f(C, a, b \ldots)$$

where $a$ and $b$ are model parameters. Among several models considered, Henry's law isotherm is the simplest one which linearly relates the adsorbed and free gas concentrations, i.e., $C_\mu = aC$. It is not commonly used for the gas–matrix systems due to its linearity, although, it has found some applications in theoretical description of complex systems (Ruckenstein et al. 1971; Smith and Williams 1984; Alvarado et al. 1998) due to its simplicity. Instead, the Langmuir isotherm has been extensively considered: $C_\mu = abC/(1 + aC)$. In this case, $a$ is the Langmuir equilibrium constant and $b$ represents complete monolayer coverage of the open surface by the gas molecules. The relationship is derived from both kinetic and statistical mechanical points of view under the assumptions of adsorption on a fixed number of sites that are energetically equivalent, and of absence of lateral interactions between the adsorbed molecules on neighboring sites. It represents a special form of the multi-layer BET adsorption equation, $C_\mu = abC/[(1 - b)(1 + b(C - 1)]$. There have been several attempts to develop isotherms based on the so-called pore filling theory (Dubinin 1966), a common form of which is the Dubinin–Astakhov equation $C_\mu = \phi \exp[-ab \ln(1/b)]/(1 - \phi)$, where now $b$ appears as a structural parameter for the surface heterogeneity.

Based on experimental observations using electron microscopy or from the analysis of the adsorption equilibrium data or the observation of the desorption behavior, Do and Wang (1998) argued that simple equilibrium isotherms may not represent the dynamics between the free and adsorbed phases in low-porosity heterogeneous materials such as activated carbon. They argued that the semi-liquid adsorption layer on the internal surfaces of the porous structure is in fact quite heterogeneous, leading to desorption time scales that are longer than the characteristic adsorption time. Hence, the desorption curve often exhibits a long

tail, indicating the presence of high-energy sites releasing the adsorbed molecules at a much lower rate. Thus, although commonly used, the assumption of instantaneously available gas at the pore walls may not be suitable. Instead, ideally, the use of an adsorption kinetics model with finite time scales for both adsorption and desorption rates is desired.

When single-component sorption rates are considered, it is common to assume that sorption follows the so-called Langmuir kinetics with adsorption and desorption rates described as follows:

$$R_{\text{ads}} = k_{\text{a}} C (C_{\mu s} - C_{\mu}) \tag{1}$$

$$R_{\text{des}} = k_{\text{d}} C_{\mu} \tag{2}$$

where the rates are in moles per unit volume of adsorbed gas per unit time with the adsorption and desorption rate coefficients, $k_{\text{a}}$ and $k_{\text{d}}$, respectively. These coefficients are a measure of the rates of collision and desorption of gas molecule to the available adsorption sites and are commonly considered to be the functions of interaction energy, $E$, between the gas molecules and the solid sites. The difference between the adsorption and desorption rates gives the net rate:

$$R_{\text{net}} = k_{\text{a}} (C_{\mu s} - C_{\mu}) C - k_{\text{d}} C_{\mu} \tag{3}$$

Consequently, in the absence of a transport mechanism of the adsorbed gas (e.g., surface diffusion), the rate of interchange between the adsorbed and free gas can be described using the following mass balance:

$$\frac{\partial C_{\mu}}{\partial t} = k_{\text{a}} (C_{\mu s} - C_{\mu}) C - k_{\text{d}} C_{\mu} \tag{4}$$

Note that, when equilibrium is reached, $R_{\text{net}} = 0$ is observed. Hence, Langmuir equilibrium isotherm is obtained with $a = k_{\text{a}}/k_{\text{d}}$, $b = C_{\mu s}$. Others used a linear approach for the adsorption kinetics of fluids in porous media, see, for example, Brusseau et al. (1991), Hu et al. (1995) and Alvarado et al. (1998), assuming that the adsorption rate is independent of the adsorbed gas concentration. Hence, the following is suggested:

$$R_{\text{ads}} = k_{\text{a}} (C_{\mu s} - C_{\mu}) C \cong k_{\text{f}} C \tag{5}$$

$$R_{\text{des}} = k_{\text{r}} C_{\mu} \tag{6}$$

Rate of the interchange between the adsorbed and free gas phases then becomes:

$$\frac{\partial C_{\mu}}{\partial t} = k_{\text{f}} C - k_{\text{r}} C_{\mu} \tag{7}$$

which can be written in the following form

$$\frac{\partial C_{\mu}}{\partial t} = k_{\text{r}} (K C - C_{\mu}) \tag{8}$$

Here, $K = k_{\text{f}}/k_{\text{r}}$ is often referred to as the equilibrium partition (or, distribution) coefficient, and $k_{\text{f}}$ and $k_{\text{r}}$ are the coefficients of forward and reverse adsorption kinetics, respectively. When the equilibrium is reached, Eq. 8 reduces to Henry's law isotherm where $a$ is defined as $K$.

Figure 1 compares numerical results of gas release from a matrix block using the linear kinetics and equilibrium adsorption models (there will be further discussion on the nature of partial differential equations solved later on). It shows the two linear isotherms constructed by periodically measuring the free and adsorbed gas concentrations in discreet time steps at the center of a matrix block. When the gas desorption rate coefficient is large (left figure

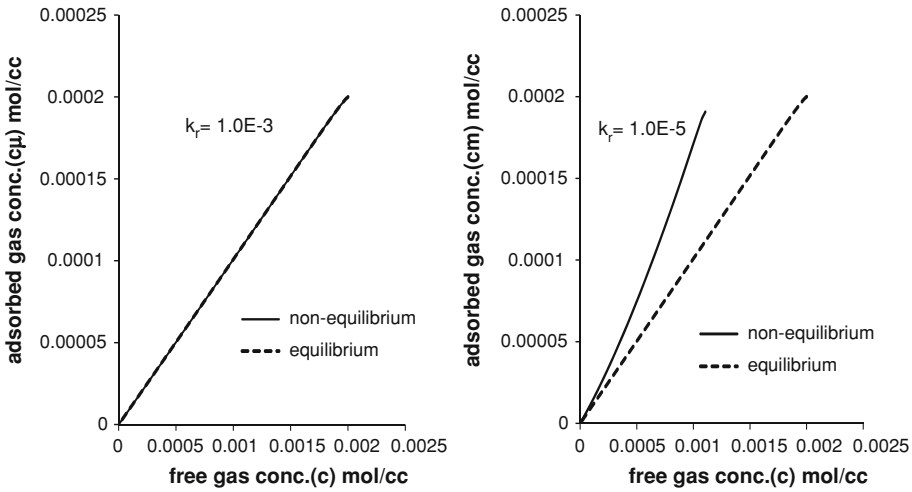


**Fig. 1** Effect of sorption kinetics on gas behavior in homogeneous porous medium. Free gas versus adsorbed gas concentrations during gas release at the center of a matrix block (1-D slab) with 10 cm. half-length, $K = 0.1$, $D = 1.0\text{E}{-3}\ \text{cm}^2/\text{s}$, $B_0 = 4.934\text{E}{-14}\,\text{cm}^2$, $\mu_g = 2.0\text{E}{-7}\,\text{kg/cm s}$, $T = 293.15\,\text{K}$, $\partial C(x = 0, t)/\partial x = \partial C_\mu(x = 0, t)/\partial x = 0.0$, and $C(x = L, t) = C_\mu(x = L, t) = 0.0$

with $k_\text{r} = 1.0\text{E} - 3$), the kinetics model maintains the same straight line relationship between the adsorbed and free gas as in the equilibrium case. When the rate coefficient is not large enough (right figure with $k_\text{r} = 1.0\text{E} - 5$); however, the isotherm corresponding to the kinetics model deviates from the equilibrium and becomes rather steep. Consequently, the domain of free gas amount is decreased, whereas the range of adsorbed gas amount is the same. Both kinetics and equilibrium cases are passing through the origin; however, in this case, the kinetics model is not following a straight line relationship between the free and adsorbed gas amounts.

As mentioned, the sorption rate coefficients are functions of interaction energy $E$. Furthermore, in the case of adsorption in porous medium, the energy itself is a function of the characteristic pore size, i.e., $E(r)$ with the pore half-width $r$. Jagiello et al. (1995) showed that the energy tends to be larger in smaller pores than in larger pores, i.e., $\text{d}E/\text{d}r < 0$. Hence, through the energy dependence of the partition coefficient, the adsorption kinetics is closely tied to the pore sizes of the matrix. This dependence is necessary in order to carry the kinetics information of the gas–solid system at the pore scale to a local continuum scale and could be explained as follows. Assume that the adsorption rate coefficient $k_\text{f}$ is independent of the interaction energy and hence its value is dictated only by the rate of collision of molecules to the surface. However, the desorption rate coefficient, $k_\text{r}$, is allowed to follow an Arrhenius relation:

$$k_\text{r} = k_{\text{r},\infty} \exp\left(\frac{-E}{RT}\right)$$

Then the partition coefficient is written in terms of the interaction energy as follows:

$$K(E) = \frac{k_\text{f}(E)}{k_\text{r}(E)} = \frac{k_\text{f}}{k_{\text{r},\infty}} \exp\left[\frac{E(r)}{RT}\right] \tag{9}$$

Now, using this definition, we take the derivative of the partition coefficient with respect to the pore size, $r$, and obtain

$$\frac{\mathrm{d}K}{\mathrm{d}r} = \frac{k_\mathrm{f}}{k_{\mathrm{r},\infty}RT} \exp\left[\frac{E(r)}{RT}\right] \frac{\mathrm{d}E(r)}{\mathrm{d}r} < 0 \tag{10}$$

Thus, we find that the changes in the partition coefficient is inversely proportional to the pore size of the matrix. This condition plays an important role in our investigation as we assume the presence of a direct coupling between the average pore size and the porosity values. Hence, we shall consider that the coefficient varies in a similar manner with the changes in porosity, i.e., $\mathrm{d}K/\mathrm{d}\phi < 0$.

### 2.2 Conservation of Gas Mass in Porous Media

In this article, the mass balance involves the following transient equations for the free and adsorbed gas amounts, where adsorption of free gas in the matrix and desorption is represented by a finite mass interchange between free and adsorbed gas.

$$\begin{aligned} \phi\frac{\partial C}{\partial t} + (1-\phi)\frac{\partial C_\mu}{\partial t} &= \frac{\partial}{\partial x}\left(\phi\, D\frac{\partial C}{\partial x}\right) + \frac{\partial}{\partial x}\left(\phi C\frac{B_0}{\mu}\frac{\partial p}{\partial x}\right) \\ \frac{\partial C_\mu}{\partial t} &= k_\mathrm{r}(KC - C_\mu) \end{aligned} \tag{11}$$

Here, $x$–$t$ are the space–time coordinates, $C(x,t)$ the free gas concentration (mol/pore volume), $C_\mu(x,t)$ the adsorbed gas concentration (mol/solid volume), $\phi$ the interconnected porosity, $D(\phi)$ the tortuosity-corrected coefficient of molecular diffusion, $B_0$ the absolute permeability of the porous medium, $p$ the pore pressure, and $\mu$ the dynamic gas viscosity. Note that the formulation contains a diffusive transport term which is Fickian in nature. This roughly corresponds to bulk (pore) diffusion as the mechanism of transport. The existence of other mechanisms (e.g., Knudsen and surface diffusion) will not be considered in this study.

The formulation is different from the case where the solid material is considered to be in equilibrium with the gas in-place, i.e., the equilibrium adsorption dynamics. We introduce virial equation of state:

$$p = RTC + RTXC^2 + RTX_1C^3 + RTX_2C^4 + \cdots. \tag{12}$$

with the parameters $X, X_1, X_2, \ldots$ representing the second, third, fourth,... virial coefficients, which are functions of temperature and composition. For practical purposes, it is common to use only the lower order terms of the equation:

$$p \cong RTC + RTXC^2 \tag{13}$$

Taking derivative of pressure with respect to the concentration and using the chain rule, Eq. 11 becomes:

$$\begin{aligned} \phi\frac{\partial C}{\partial t} + (1-\phi)\frac{\partial C_\mu}{\partial t} &= \frac{\partial}{\partial x}\left[\phi\left(D + C\frac{B_0RT}{\mu}(2XC+1)\right)\frac{\partial C}{\partial x}\right] \\ \frac{\partial C_\mu}{\partial t} &= k_\mathrm{r}(KC - C_\mu) \end{aligned} \tag{14}$$

We performed sensitivity analysis using methane with a coal sample to determine the effect of ideal gas assumption (with $XC = 0$) on the gas–matrix system (Fig. 2). The ideal gas assumption does not create significant effects, and it has no impact on the concentration

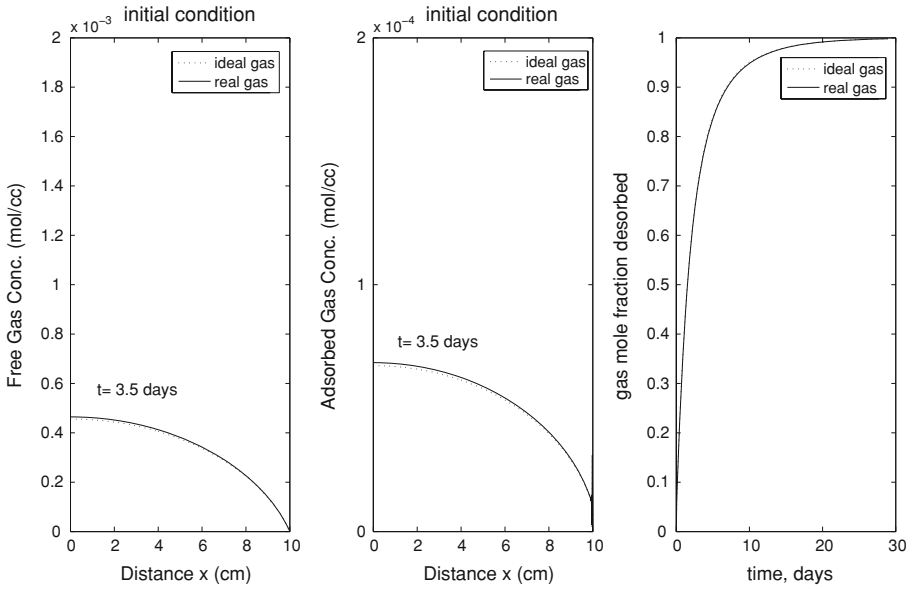


**Fig. 2** Comparison of ideal and real gas models. *Left* Free gas concentration profile versus distance from the center of coal matrix. *Middle* Adsorbed gas concentration profile versus distance from the center of coal matrix. *Right* Gas mole fraction desorbed versus time. Considered gas is methane and the half length of the matrix block (1-D slab) is 10 cm, $k_r = 1.0E-5\,s^{-1}$, $K = 0.1$, $D = 1.0E{-}3\,cm^2/s$, $B_0 = 4.934E{-}14\,cm^2$, $\mu_g = 2.0E{-}7\,kg/cm\,s$, $T = 293.15\,K$, $\partial C(x=0,t)/\partial x = \partial C_\mu(x=0,t)/\partial x = 0.0$ and $C(x=L,t) = C_\mu(x=L,t) = 0.0$

profiles and on the fractional gas recovery curve. The following governing equation for the ideal free gas mass will thus be adopted for simplicity in our analysis:

$$\begin{aligned} \phi\frac{\partial C}{\partial t} + (1-\phi)\frac{\partial C_\mu}{\partial t} &= \frac{\partial}{\partial x}\left[\phi\left(D + C\frac{B_0 RT}{\mu}\right)\frac{\partial C}{\partial x}\right] \\ \frac{\partial C_\mu}{\partial t} &= k_r(KC - C_\mu) \end{aligned} \tag{15}$$

Next, Eq. 15 is reorganized and written in the following form:

$$\begin{aligned} \frac{\partial C}{\partial t} = D\frac{\partial^2 C}{\partial x^2} + \alpha\frac{\partial C}{\partial x} + \beta\alpha'\frac{\partial C}{\partial x} + \beta C\frac{\partial^2 C}{\partial x^2} - \Phi k_r(KC - C_\mu) \\ \frac{\partial C_\mu}{\partial t} = k_r(KC - C_\mu) \end{aligned} \tag{16}$$

Here, we introduce $\alpha = \partial(\phi D)/\phi\partial x$ as an effective drift velocity, reflecting changes in free gas concentration due to a non-constant diffusivity with a gradient. In addition, we have $\alpha' = \partial(\phi C)/\phi\partial x$, and we introduce, $\Phi = (1-\phi)/\phi$ as the solid-to-bulk volume ratio, $\beta = B_0 RT/\mu$ as the gas mobility.

Prior to the analysis of gas behavior in heterogeneous porous medium, it is worthwhile to briefly mention here the impact of outer boundary (i.e., the pressure condition in the surrounding fractures) on the ultimate gas recovery using Eq. 16. Figure 3 depicts the effect of outer boundary condition which will be used in our numerical simulation. The initially available free gas release takes place rapidly within a few days for all the cases considered. Following the completion of free gas release, the desorbed gas becomes the main source of

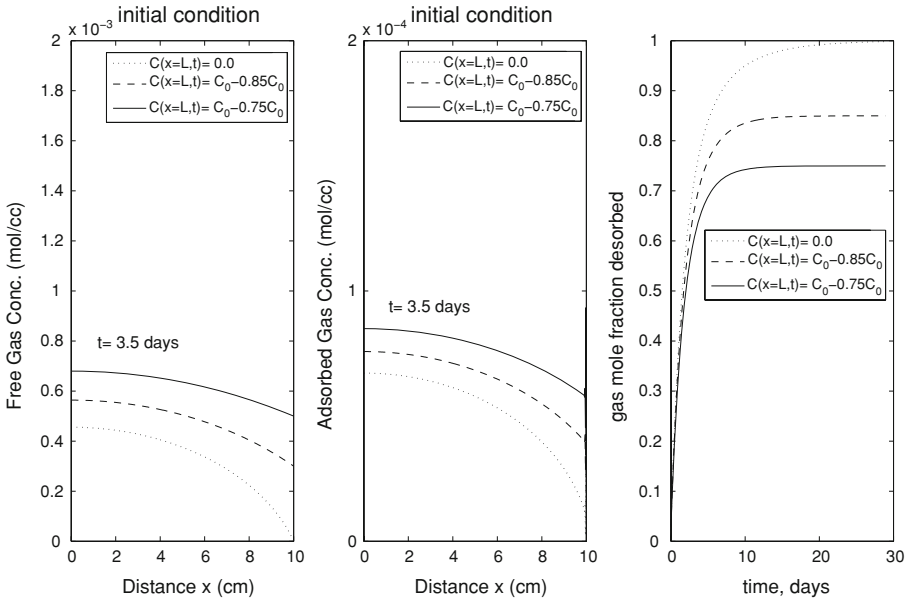


**Fig. 3** Influence of outer boundary condition on the ultimate gas recovery from a matrix block surrounded by fractures. *Left* Free gas concentration profile versus distance from the center of matrix. *Middle* Adsorbed gas concentration profile versus distance from the center of matrix. *Right* Gas mole fraction desorbed versus time. The half-length of the matrix block (1-D slab) is 10 cm, $k_r = 1.0\text{E}{-5}\,\text{s}^{-1}$, $K = 0.1$, $D = 1.0\text{E}{-3}\,\text{cm}^2/\text{s}$, $B_0 = 4.934\text{E}{-14}\,\text{cm}^2$, $\mu_g = 2.0\text{E}{-7}\,\text{kg/cm s}$, $T = 293.15\,\text{K}$, $\partial C(x=0,t)/\partial x = \partial C_\mu(x=0,t)/\partial x = 0.0$, and $C_\mu(x=L,t) = 0.0$. The initial pore pressure is 4874.6 kPa

production. During this latter period, the gas release is slow and a relatively long period of time is required for the ultimate gas recovery. In the case of zero partial pressure of methane at the outer boundary (i.e., ideal but unrealistic case of removing the released gas), complete recovery is achieved. However, when the partial pressure of methane at the boundary is increased to a finite value, which means less pressure drop across the coal matrix, the results show that the gas release rate is lower and the ultimate gas recovery is less than unity. Here, we assumed fixed outer boundary conditions which are equal to 15% and 25% of the initially distributed free gas in the matrix. In the following analysis, the outer boundary of the matrices will be fixed to a constant value.

## 3 Gas Behavior in Heterogeneous Matrix

In our naturally occurring porous medium, heterogeneity is represented by a time-independent, spatially variable random porosity field $\phi = \bar{\phi} + \tilde{\phi}$ in terms of its mean $\bar{\phi}$ and small fluctuation $\tilde{\phi}$. Further, it is considered that the matrix porosity obeys stationarity of moments of order one and two (mean and the variance of porosity kept constant) with a well-defined spatial covariance function. All the dependent variables, transport and rate coefficients are affected by the medium heterogeneity presented by the porosity random field; therefore, they are also considered to be random variables. Consider that an over-bar and a tilde over a quantity denote its average value and its fluctuations about the mean, respectively. We then have:

$$\begin{aligned}
\alpha &= \bar{\alpha} + \tilde{\alpha} \\
\alpha' &= \bar{\alpha}' + \tilde{\alpha}' \\
C &= \bar{C} + \tilde{C} \\
C_\mu &= \bar{C}_\mu + \tilde{C}_\mu \\
D &= \bar{D} + \tilde{D} \\
\Phi &= \bar{\Phi} + \tilde{\Phi} \\
K &= \bar{K} + \tilde{K}
\end{aligned}$$

Note here that the partition coefficient $K$ is also considered as a random variable so that the porosity fluctuations have the potential to create variations in gas adsorption and desorption rates. This is a reasonable and important approach since coals and shales are mixtures of various minerals and organic material exhibiting an intricate pore network. Variations in the material properties (e.g., rank and maceral content) add to structurally complex nature of coals and shales, which influences the gas retention (adsorption) capacity. Substituting these expressions into the governing gas mass equation (16), and taking the expectation, the mass balance equation for mean free and adsorbed gas concentrations are obtained.

$$\begin{aligned}
&\frac{\partial \bar{C}}{\partial t} + \bar{\Phi}\frac{\partial \bar{C}_\mu}{\partial t} - \bar{D}\frac{\partial^2 \bar{C}}{\partial x^2} = \bar{R} \\
&\frac{\partial \bar{C}_\mu}{\partial t} = k_{\mathrm{r}}\left(\bar{K}\bar{C} + \overline{\tilde{K}\tilde{C}} - \bar{C}_\mu\right)
\end{aligned} \tag{17}$$

Subtracting the obtained mean equations from the original ones (i.e., Eq. 16), the mean removed equations are derived as following:

$$\begin{aligned}
&\frac{\partial \tilde{C}}{\partial t} + \bar{\Phi}\frac{\partial \tilde{C}_\mu}{\partial t} - \bar{\alpha}\frac{\partial \tilde{C}}{\partial x} - \bar{D}\frac{\partial^2 \tilde{C}}{\partial x^2} - \beta\bar{\alpha}'\frac{\partial \tilde{C}}{\partial x} - \beta\bar{C}\frac{\partial^2 \tilde{C}}{\partial x^2} - \beta\tilde{C}\frac{\partial^2 \bar{C}}{\partial x^2} = \tilde{R} \\
&\frac{\partial \tilde{C}_\mu}{\partial t} + k_{\mathrm{r}}\tilde{C}_\mu = k_{\mathrm{r}}\left(\overline{K\tilde{C}} + \tilde{K}\bar{C} + \tilde{K}\tilde{C} - \overline{\tilde{K}\tilde{C}}\right)
\end{aligned} \tag{18}$$

where we defined $\bar{R}$ and $\tilde{R}$ as

$$\bar{R} = \bar{\alpha}\frac{\partial \bar{C}}{\partial x} + \beta\bar{\alpha}'\frac{\partial \bar{C}}{\partial x} + \beta\bar{C}\frac{\partial^2 \bar{C}}{\partial x^2} + \overline{\tilde{\alpha}\frac{\partial \tilde{C}}{\partial x}} + \overline{\tilde{D}\frac{\partial^2 \tilde{C}}{\partial x^2}} + \beta\overline{\tilde{\alpha}'\frac{\partial \tilde{C}}{\partial x}} - \overline{\tilde{\Phi}\frac{\partial \tilde{C}_\mu}{\partial t}} \tag{19}$$

$$\begin{aligned}
\tilde{R} = &-\tilde{\Phi}\frac{\partial \bar{C}_\mu}{\partial t} - \tilde{\Phi}\frac{\partial \tilde{C}_\mu}{\partial t} + \overline{\tilde{\Phi}\frac{\partial \tilde{C}_\mu}{\partial t}} + \tilde{\alpha}\frac{\partial \bar{C}}{\partial x} + \tilde{\alpha}\frac{\partial \tilde{C}}{\partial x} - \overline{\tilde{\alpha}\frac{\partial \tilde{C}}{\partial x}} + \tilde{D}\frac{\partial^2 \bar{C}}{\partial x^2} + \tilde{D}\frac{\partial^2 \tilde{C}}{\partial x^2} - \overline{\tilde{D}\frac{\partial^2 \tilde{C}}{\partial x^2}} \\
&+ \beta\tilde{\alpha}'\frac{\partial \bar{C}}{\partial x} + \beta\tilde{\alpha}'\frac{\partial \tilde{C}}{\partial x} - \beta\overline{\tilde{\alpha}'\frac{\partial \tilde{C}}{\partial x}} + \beta\tilde{C}\frac{\partial^2 \tilde{C}}{\partial x^2} - \beta\overline{\tilde{C}\frac{\partial^2 \tilde{C}}{\partial x^2}}
\end{aligned} \tag{20}$$

Next, we implement the assumption of small-perturbations. Accordingly, the porosity fluctuations are so small that the terms including fluctuation correlations higher than second order are neglected. In homogeneous porous media, $\bar{\alpha}$, and $\bar{\alpha}'$ are defined as (L'Heureux 2004)

$$\begin{aligned}
\bar{\alpha} &\cong \overline{\tilde{D}\frac{\partial \tilde{\phi}}{\partial x}} - \left(\frac{\bar{D}}{\bar{\phi}}\right)\overline{\tilde{\phi}\frac{\partial \tilde{\phi}}{\partial x}} \\
\bar{\alpha}' &\cong \overline{\tilde{C}\frac{\partial \tilde{\phi}}{\partial x}} - \left(\frac{\bar{C}}{\bar{\phi}}\right)\overline{\tilde{\phi}\frac{\partial \tilde{\phi}}{\partial x}}
\end{aligned}$$

which are already second order in porosity fluctuations; therefore, $\bar{\alpha}\partial\tilde{C}/\partial x \cong 0$ and $\bar{\alpha'}\partial\tilde{C}/\partial x \cong 0$ are taken.

Introducing the notation of $\xi_1 = \tilde{\alpha}$ and $\xi_2 = \tilde{D}$ and taking space-Fourier and time-Laplace transform of the Eq. 17 leads to Fourier–Laplace solution of the mean concentrations:

$$\begin{aligned}(s + k^2\bar{D})\bar{C}_{ks} - \bar{C}_{k,t=0} + s\bar{\Phi}(\bar{C}_\mu)_{ks} - \bar{\Phi}(\bar{C}_\mu)_{k,t=0} &= \bar{R}_{ks} \\ (\bar{C}_\mu)_{ks} = (s + k_\mathrm{r})^{-1}\left[(\bar{C}_\mu)_{k,t=0} + k_\mathrm{r}(\bar{K}\bar{C} + \overline{\tilde{K}\tilde{C}})_{ks}\right]\end{aligned} \tag{21}$$

where $k$ is the wave number, $s$ the Laplace transform variable, $\bar{C}_{k,t=0}$ and $(\bar{C}_\mu)_{k,t=0}$ are the Fourier transforms of the initial mean concentration of free and adsorbed gas, respectively. Here $\bar{R}_{ks}$ is defined as

$$\bar{R}_{ks} = \left(\bar{\alpha}\frac{\partial\bar{C}}{\partial x} + \beta\bar{\alpha}'\frac{\partial\bar{C}}{\partial x} + \beta\bar{C}\frac{\partial^2\bar{C}}{\partial x^2} + \sum_{m=1,2}\overline{\frac{\xi_m\partial^m\tilde{C}}{\partial x^m}} + \beta\overline{\frac{\tilde{\alpha}'\partial\tilde{C}}{\partial x}} - \overline{\frac{\tilde{\Phi}\partial\tilde{C}_\mu}{\partial t}}\right)_{ks} \tag{22}$$

First and second terms in Eq. 22 are corrections to drift velocity, the third term is related to diffusive transport, and the last three terms indicate non-trivial cross-correlations between the fluctuating porosity, transport, and kinetic coefficients with free and adsorbed gas concentration fields. Combining conservation of gas mass equation (21) for the free and adsorbed gas we have:

$$\left[s\left(1 + \frac{\bar{\Phi}k_\mathrm{r}\bar{K}}{s + k_\mathrm{r}}\right) + k^2\bar{D}\right]\bar{C}_{ks} = \bar{C}_{k,t=0} + \left(\bar{\Phi} - \frac{s\bar{\Phi}}{s + k_\mathrm{r}}\right)\bar{C}_{\mu k,t=0} - \frac{s\bar{\Phi}k_\mathrm{r}}{s + k_\mathrm{r}}\left(\overline{\tilde{K}\tilde{C}}\right)_{ks} + \bar{R}_{ks}$$

Hence, formal solution of the Fourier–Laplace transform of the mean concentration $\bar{C}_{ks}$ is

$$\bar{C}_{ks} = \hat{G}_{ks}^{-1}\cdot\bar{R}_{ks} + \hat{G}_{ks}^{-1}\cdot\mathrm{X}_{ks} \tag{23}$$

where $\hat{G}_{ks}$ and $\mathrm{X}_{ks}$ are defined as

$$\begin{aligned}\hat{G}_{ks} &= \left[s\left(1 + \frac{\bar{\Phi}k_\mathrm{r}\bar{K}}{s + k_\mathrm{r}}\right) + k^2\bar{D}\right] \\ \mathrm{X}_{ks} &= \left[\bar{C}_{k,t=0} + \left(\bar{\Phi} - \frac{s\bar{\Phi}}{s + k_\mathrm{r}}\right)(\bar{C}_\mu)_{k,t=0} - \frac{s\bar{\Phi}k_\mathrm{r}}{s + k_\mathrm{r}}\left(\overline{\tilde{K}\tilde{C}}\right)_{ks}\right]\end{aligned}$$

In order to find the equivalent expression for free gas fluctuation $\tilde{C}$ in Fourier–Laplace domain, first we need to use the mean-field approximation for the terms $\beta\bar{C}\partial^2\tilde{C}/\partial x^2$ and $\beta\tilde{C}\partial^2\bar{C}/\partial x^2$. Assuming the average concentration is replaced by its value averaged over a large space domain $L$ and time interval $\tau$: $\bar{\tilde{C}} = \int_0^\tau\int_0^L C(x,t)\mathrm{d}x\mathrm{d}t/L\tau \equiv g$ and $\partial\bar{\tilde{C}}/\partial\bar{\phi} = g'$. Equivalently, we take $\bar{C}_{ks} = g$ in Fourier–Laplace domain. Figure 4 shows the effect of tight matrix porosity on the mean-field approximation of free gas concentration $g$ and its derivative $g'$.

Next, we apply Fourier–Laplace transform to the perturbation equation (18):

$$\begin{aligned}\left(s + k^2\bar{D} + 2\beta g k^2\right)\tilde{C}_{ks} + \bar{\Phi}s\tilde{C}_{\mu ks} &= \tilde{R}_{ks} \\ \tilde{C}_{\mu ks} = (k_\mathrm{r} + s)^{-1}k_\mathrm{r}\bar{K}\tilde{C}_{ks} + (k_\mathrm{r} + s)^{-1}k_\mathrm{r}&\left[\tilde{K}\bar{C} + \tilde{K}\tilde{C} - \overline{\tilde{K}\tilde{C}}\right]_{ks}\end{aligned} \tag{24}$$

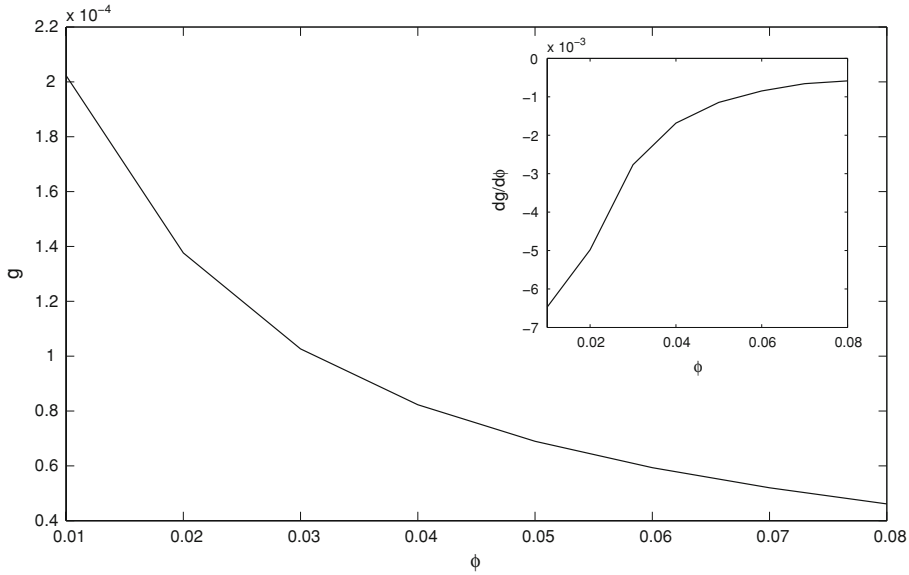


**Fig. 4** Effect of tight matrix porosity on the mean field approximation of free gas concentration, $g$ and its derivative $g'$. $k_r = 1.0\text{E}{-5}\,\text{s}^{-1}$, $K = 0.1$, $D = 1.0\text{E}{-3}\ \text{cm}^2/\text{s}$, $B_0 = 4.934\text{E}{-14}\,\text{cm}^2$, $\mu_g = 2.0\text{E}{-7}\,\text{kg/cm s}$, $T = 293.15\,\text{K}$, $\partial C(x=0,t)/\partial x = \partial C_\mu(x=0,t)/\partial x = 0.0$, and $C(x=L,t) = C_\mu(x=L,t) = 0.0$

where $\tilde{R}_{ks}$ is defined as

$$\tilde{R}_{ks} = \left( \begin{array}{l} -\tilde{\Phi}\dfrac{\partial \bar{C}_\mu}{\partial t} - \bar{\Phi}\dfrac{\partial \tilde{C}_\mu}{\partial t} + \overline{\dfrac{\tilde{\Phi}\partial \tilde{C}_\mu}{\partial t}} + \tilde{\alpha}\dfrac{\partial \bar{C}}{\partial x} + \bar{\alpha}\dfrac{\partial \tilde{C}}{\partial x} - \overline{\dfrac{\tilde{\alpha}\partial \tilde{C}}{\partial x}} + \bar{D}\dfrac{\partial^2 \bar{C}}{\partial x^2} + \tilde{D}\dfrac{\partial^2 \bar{C}}{\partial x^2} \\ -\overline{\dfrac{\tilde{D}\partial^2 \tilde{C}}{\partial x^2}} + \beta\tilde{\alpha}'\dfrac{\partial \bar{C}}{\partial x} + \beta\bar{\alpha}'\dfrac{\partial \tilde{C}}{\partial x} - \beta\overline{\dfrac{\tilde{\alpha}'\partial \tilde{C}}{\partial x}} + \beta\tilde{C}\dfrac{\partial^2 \bar{C}}{\partial x^2} - \beta\overline{\dfrac{\tilde{C}\partial^2 \tilde{C}}{\partial x^2}} \end{array} \right)_{ks} \tag{25}$$

In the derivation of Eq. 8, terms of higher order than quadratic are neglected, whereas $\tilde{C}(x,0) = \tilde{C}_\mu(x,0) = 0$ are considered. Combining the free and adsorbed gas fluctuation equations in (24) gives

$$\left[ s\left(1 + \frac{\bar{\Phi}k_r\bar{K}}{s+k_r}\right) + (\bar{D} + 2\beta g)k^2 \right] \tilde{C}_{ks} = \tilde{R}_{ks} - \frac{s\bar{\Phi}k_r}{s+k_r}\left[\tilde{K}\bar{C} + \bar{K}\tilde{C} - \overline{\tilde{K}\tilde{C}}\right]_{ks}$$

Hence, the formal solution to the Fourier–Laplace transform of the concentration fluctuation $\tilde{C}_{ks}$ is given by

$$\tilde{C}_{ks} = G_{ks}^{-1}\tilde{R}_{ks} - L_{ks}M_{ks} \tag{26}$$

in which

$$G_{ks} = \left[ s\left(1 + \frac{\bar{\Phi}k_r\bar{K}}{s+k_r}\right) + (\bar{D} + 2\beta g)k^2 \right]_{ks}$$

$$L_{ks} = \left(\frac{s\bar{\Phi}k_r}{s+k_r}\right) G_{ks}^{-1}$$

$$M_{ks} = \left[\tilde{K}\bar{C} + \bar{K}\tilde{C} - \overline{\tilde{K}\tilde{C}}\right]_{ks}$$

In the space–time domain, the fluctuating concentration field is given by the convolution integral

$$\begin{aligned}\tilde{C}(x,t) &= \int_0^t \int G^{-1}\left(x-x',t-t'\right)\tilde{R}\left(x',t'\right)\mathrm{d}x'\mathrm{d}t' \\ &\quad - \int_0^t \int L\left(x-x',t-t'\right)M\left(x',t'\right)\mathrm{d}x'\mathrm{d}t' \\ &\equiv G^{-1}_{x-x',t-t'} * \tilde{R}_{x',t'} - L_{x-x',t-t'} * M_{x',t'} \end{aligned} \tag{27}$$

Substituting $\tilde{C}$ in adsorbed gas fluctuation equation gives

$$\begin{aligned}(\tilde{C}_\mu)_{ks} &= (k_\mathrm{r}+s)^{-1}k_\mathrm{r}\bar{K}\tilde{C}_{ks} + (k_\mathrm{r}+s)^{-1}k_\mathrm{r}\left[\tilde{K}\bar{C}+\tilde{K}\tilde{C}-\overline{\tilde{K}\tilde{C}}\right]_{ks} \\ (\tilde{C}_\mu)_{ks} &= (k_\mathrm{r}+s)^{-1}k_\mathrm{r}\bar{K}\left(G^{-1}_{ks}\cdot\tilde{R}_{ks} - L_{ks}\cdot M_{ks}\right) + (k_\mathrm{r}+s)^{-1}k_\mathrm{r}\left[\tilde{K}\bar{C}+\tilde{K}\tilde{C}-\overline{\tilde{K}\tilde{C}}\right]_{ks} \\ &= \breve{G}^{-1}_{ks}\tilde{R}_{ks} + \breve{L}_{ks}M_{ks} \end{aligned} \tag{28}$$

in which $\breve{G}^{-1}_{ks} = \left(\frac{\bar{K}k_\mathrm{r}}{s+k_\mathrm{r}}\right)G^{-1}_{ks}$ and $\breve{L}_{ks} = \left(\frac{-\bar{K}k_\mathrm{r}}{s+k_\mathrm{r}}L_{ks} + \frac{k_\mathrm{r}}{s+k_\mathrm{r}}\right)$.

In the space–time domain, the fluctuating adsorbed gas concentration field is given by the convolution integral

$$\begin{aligned}\tilde{C}_\mu(x,t) &= \int_0^t \int \breve{G}^{-1}\left(x-x',t-t'\right)\tilde{R}\left(x',t'\right)\mathrm{d}x'\mathrm{d}t' \\ &\quad - \int_0^t \int \breve{L}\left(x-x',t-t'\right)M\left(x',t'\right)\mathrm{d}x'\mathrm{d}t' \\ &\equiv \breve{G}^{-1}_{x-x',t-t'} * \tilde{R}_{x',t'} - \breve{L}_{x-x',t-t'} * M_{x',t'} \end{aligned} \tag{29}$$

The cross-correlation terms in Eq. 22, i.e., the last three terms, are obtained using $\tilde{C}$ and $\tilde{C}_\mu$. The summation term can be obtained by multiplying the proper spatial derivative of the concentration fluctuation, $\tilde{C}$, with the fluctuating transport term, $\xi_m(x)$, neglecting the third-order porosity fluctuation terms and taking the expectation.

$$\sum_{m=1,2}\frac{\overline{\xi_m\partial^m\tilde{C}}}{\partial x^m} = \sum_{m=1,2}\frac{\partial^m G^{-1}_{x-x',t-t'}}{\partial x^m} * \overline{\xi_m\tilde{R}_{x',t'}} - \sum_{m=1,2}\frac{\partial^m L_{x-x',t-t'}}{\partial x^m} * \overline{\xi_m M_{x'},t'} \tag{30}$$

The fourth term in Eq. 22 is obtained similarly using the definition of $\tilde{C}$:

$$\beta\frac{\overline{\tilde{\alpha}'\partial\tilde{C}}}{\partial x} = \frac{\partial G^{-1}_{x-x',t-t'}}{\partial t} * \beta\overline{\tilde{\alpha}'\tilde{R}} - \frac{\partial L_{x-x',t-t'}}{\partial t} * \beta\overline{\tilde{\alpha}'M} \tag{31}$$

And the last term is obtained by multiplying the time derivative of the adsorbed gas concentration fluctuation, $\tilde{C}_\mu$, with $\tilde{\Phi}$ and taking the average over realizations.

$$\frac{\overline{\tilde{\Phi}\partial\tilde{C}_\mu}}{\partial t} = \frac{\partial\breve{G}^{-1}_{x-x',t-t'}}{\partial t} * \overline{\tilde{\Phi}\tilde{R}} + \frac{\partial\breve{L}_{x-x',t-t'}}{\partial t} * \overline{\tilde{\Phi}M} \tag{32}$$

where the third-order terms in the porosity fluctuations have been dropped. Taking the space-Fourier and time-Laplace transformation of Eqs. (30)–(32) give

$$\sum_{m=1,2} \overline{\frac{\xi_m \partial^m \tilde{C}}{\partial x^m}} = P_{ks}\bar{C}_{\mu k,t=0} + Q_{ks}\bar{C}_{ks} + S_{ks}\bar{C}_{ks} - T_{ks}\bar{C}_{ks} \tag{33}$$

$$\beta \overline{\frac{\tilde{\alpha}'\partial \tilde{C}}{\partial x}} = U_{ks}\bar{C}_{\mu k,t=0} + V_{ks}\bar{C}_{ks} + W_{ks}\bar{C}_{ks} - Y_{ks}\bar{C}_{ks} \tag{34}$$

$$\overline{\frac{\tilde{\Phi}\partial \tilde{C}_\mu}{\partial t}} = Z_{ks}\bar{C}_{\mu k,t=0} + M_{ks}\bar{C}_{ks} + N_{ks}\bar{C}_{ks} + O_{ks}\bar{C}_{ks} \tag{35}$$

Now substituting all these equations back to Eq. 22, $\bar{R}_{ks}$ becomes

$$\begin{aligned}\bar{R}_{ks} = &\left(\bar{\alpha}\frac{\partial \bar{C}}{\partial x} + \beta\bar{\alpha}'\frac{\partial \bar{C}}{\partial x} + \beta\bar{C}\frac{\partial^2 \bar{C}}{\partial x^2}\right)_{ks} + P_{ks}\bar{C}_{\mu k,t=0} + Q_{ks}\bar{C}_{ks} + S_{ks}\bar{C}_{ks} - T_{ks}\bar{C}_{ks} \\ &+ U_{ks}\bar{C}_{\mu k,t=0} + V_{ks}\bar{C}_{ks} + W_{ks}\bar{C}_{ks} - Y_{ks}\bar{C}_{ks} + Z_{ks}\bar{C}_{\mu k,t=0} \\ &+ M_{ks}\bar{C}_{ks} + N_{ks}\bar{C}_{ks} + O_{ks}\bar{C}_{ks}\end{aligned} \tag{36}$$

where a series of integral terms appear and are tabulated in Table 2, in Appendix A. In the table, $Q$ is the dummy wave number label. In addition, we can express the cross-correlation $\overline{\tilde{K}\tilde{C}}$ in Eq. 17 using the definition of $\tilde{C}$ (Eq. 27) in the following form

$$\overline{\tilde{K}\tilde{C}} = G^{-1} * \overline{\tilde{K}\tilde{R}} - L * \overline{\tilde{K}M} \tag{37}$$

Taking space–Fourier and time–Laplace transform of Eq. 37 leads to

$$\left(\overline{\tilde{K}\tilde{C}}\right)_{ks} = I_{ks}\bar{C}_{\mu k,t=0} + E_{ks}\bar{C}_{ks} + F_{ks}\bar{C}_{ks} - J_{ks}\bar{C}_{ks} \tag{38}$$

which also includes a set of integral terms given in Table 3 in the Appendix A. In order to evaluate these integrals, the porosity fluctuations, $\tilde{\phi}$, around the mean porosity, $\bar{\phi}$, assumed to be Gaussian random variable with zero mean and variance, $\sigma_\phi^2$, and the spatial correlation function defined as $\overline{\tilde{\phi}(x)\tilde{\phi}(y)} = \sigma_\phi^2 f(|x-y|)$ are considered. The auto- and cross-covariances appearing in the integrals are defined using Gaussian correlation function and the assumption of second-order stationarity. Then $\overline{\tilde{\alpha}_x\tilde{\alpha}_{x'}} = \left(D' + \bar{D}/\bar{\phi}\right)^2 \overline{\partial_x\tilde{\phi}(x)\partial_{x'}\tilde{\phi}(x')} = -\left(D' + \bar{D}/\bar{\phi}\right)^2 \sigma_\phi^2 d^2 f(x)/\mathrm{d}x^2$ is defined in space and time domain which is $\overline{\xi_{Q1}\xi_{-Q1}} = \overline{\tilde{\alpha}_Q\tilde{\alpha}_{-Q}} = \left(D' + \bar{D}/\bar{\phi}\right)^2 \sigma_\phi^2 Q^2 f_Q$ in Fourier space domain where $\sigma_\phi^2$ is the variance of porosity, and $f_Q$ is the Fourier transform of the porosity correlation function $f(x)$. Assuming Gaussian random variable with Gaussian model of spatial covariance porosity, characterized by correlation length, $\lambda$, we have $f_x = \exp\left(-x^2/2\lambda^2\right)$ and $f_Q = \sqrt{2\pi}\lambda\exp\left(-Q^2\lambda^2/2\right)$ in the real and spectral domains, respectively. Therefore, we defined a set of auto- and cross-covariance in Table 4, Appendix B. Using conventional approximations $s = k = 0$ in $Q$-dependent terms of the integrands, the following solutions are obtained for the integrals defined in Tables 2 and 3:

$$P_{ks} = \frac{\bar{D}\sigma_\phi^2}{\bar{\phi}(\bar{D}+2\beta g)}; \quad Q_{ks} = \frac{D'\sigma_\phi^2}{(\bar{D}+2\beta g)}\left(2D' + \frac{\bar{D}}{\bar{\phi}}\right)k^2; \quad S_{ks} = T_{ks} = Y_{ks} = 0;$$

$$U_{ks} = \frac{\beta(g' + \frac{g}{\bar{\phi}})\sigma_\phi^2}{(\bar{D}+2\beta g)}; \quad V_{ks} = \frac{\beta D'\left(g' + \frac{g}{\bar{\phi}}\right)\sigma_\phi^2}{(\bar{D}+2\beta g)}k^2; \quad W_{ks} = Z_{ks} = M_{ks} = N_{ks} = 0;$$

$$O_{ks} = k_\mathrm{r}K'\sigma_\phi^2; \quad I_{ks} = -K'\sigma_\phi^2\frac{\lambda^2}{\bar{D}}; \quad F_{ks} = K'D'\sigma_\phi^2\frac{\lambda^2}{\bar{D}}k^2; \quad E_{ks} = J_{ks} = 0;$$

in which $\breve{G}^{-1}_{k(0)} = 0$ and $\breve{L}_{k(0)} = k_\mathrm{r}$. Thus, the $\bar{R}_{ks}$ becomes

$$\begin{aligned}\bar{R}_{ks} = &\left(\bar{\alpha}\frac{\partial\bar{C}}{\partial x} + \beta\bar{\alpha}'\frac{\partial\bar{C}}{\partial x} + \beta\bar{C}\frac{\partial^2\bar{C}}{\partial x^2}\right)_{ks} + \frac{\bar{D}\sigma_\phi^2}{\bar{\phi}(\bar{D}+2\beta g)}(\bar{C}_\mu)_{k,t=0}\\ &+\left(\frac{D'\sigma_\phi^2}{\bar{D}+2\beta g}\right)\left(2D' + \frac{\bar{D}}{\bar{\phi}}\right)\\ &\times k^2\bar{C}_{ks} + \frac{\beta\left(g' + g/\bar{\phi}\right)\sigma_\phi^2}{\bar{D}+2\beta g}(\bar{C}_\mu)_{k,t=0} + \frac{\beta D'\left(g' + g/\bar{\phi}\right)\sigma_\phi^2}{\bar{D}+2\beta g}k^2\bar{C}_{ks} + k_\mathrm{r}K'\sigma_\phi^2\bar{C}_{ks}\end{aligned} \tag{39}$$

Taking the inverse Laplace–Fourier transform, $\bar{R}_{ks}$ becomes:

$$\begin{aligned}\bar{R} = &\bar{\alpha}\frac{\partial\bar{C}}{\partial x} + \beta\bar{\alpha}'\frac{\partial\bar{C}}{\partial x} + \beta\bar{C}\frac{\partial^2\bar{C}}{\partial x^2}\\ &+\left(\frac{\bar{D}\sigma_\phi^2}{\bar{\phi}(\bar{D}+2\beta g)}\right)(\bar{C}_\mu)_{x,t=0} - \left(\frac{D'(2D' + \bar{D}/\bar{\phi})\sigma_\phi^2}{\bar{D}+2\beta g}\right)\frac{\partial^2\bar{C}}{\partial x^2}\\ &+\left(\frac{\beta(g' + g/\bar{\phi})\sigma_\phi^2}{(\bar{D}+2\beta g)}\right)(\bar{C}_\mu)_{x,t=0} - \left(\frac{\beta D'(g' + g/\bar{\phi})\sigma_\phi^2}{\bar{D}+2\beta g}\right)\frac{\partial^2\bar{C}}{\partial x^2} + k_\mathrm{r}K'\sigma_\phi^2\bar{C}\end{aligned} \tag{40}$$

and also $\left(\overline{\tilde{K}\tilde{C}}\right)_{ks}$ is given by:

$$\left(\overline{\tilde{K}\tilde{C}}\right)_{ks} = -\left[K'\sigma_\phi^2\lambda^2/(\bar{D}+2\beta g)\right]\bar{C}_{\mu k,t=0} + \left[K'D'\sigma_\phi^2\lambda^2/(\bar{D}+2\beta g)\right]k^2\bar{C}_{ks} \tag{41}$$

which, in the time–space domain results in:

$$\overline{\tilde{K}\tilde{C}} = -\left[K'\sigma_\phi^2\lambda^2/(\bar{D}+2\beta g)\right](\bar{C}_\mu)_{x,t=0} - \left[K'D'\sigma_\phi^2\lambda^2/(\bar{D}+2\beta g)\right]\frac{\partial^2\bar{C}}{\partial x^2} \tag{42}$$

## 4 Upscaled Governing Equations

Substituting equations (40) and (42) into the mean governing equations given in (17), using the definitions of $\bar{\alpha}$, $\bar{\alpha}'$, and $\beta$, and re-arranging these leads to the following form of the governing equations:

$$\begin{aligned}\bar{\phi}\frac{\partial\bar{C}}{\partial t} + (1-\bar{\phi})\frac{\partial\bar{C}_\mu}{\partial t} &= \frac{\partial}{\partial x}\left(\bar{\phi}\mathcal{D}\frac{\partial\bar{C}}{\partial x}\right) + \frac{\partial}{\partial x}\left(\bar{\phi}\bar{C}\frac{B_0}{\mu}\frac{\partial\bar{p}}{\partial x}\right) + \Gamma_1 + \Gamma_2\\ \frac{\partial\bar{C}_\mu}{\partial t} &= k_\mathrm{r}\left[\bar{K}\bar{C} - \left(\bar{C}_\mu + \Gamma_3\right)\right]\end{aligned} \tag{43}$$

in which new quantities reflecting the effects of local heterogeneities appear. These are defined as:

$$\mathcal{D} = \bar{D} - D'\sigma_\phi^2 \left( \frac{2D' + \beta g' + \dfrac{\bar{D} + \beta g}{\bar{\phi}}}{\bar{D} + 2\beta g} \right) \tag{44}$$

$$\Gamma_1 = \left[ \bar{D} + \beta(\bar{\phi} g' + g) \right] \frac{\sigma_\phi^2 \bar{C}_{\mu 0}}{(\bar{D} + 2\beta g)} \tag{45}$$

$$\Gamma_2 = k_\mathrm{r} K' \bar{\phi} \sigma_\phi^2 \bar{C} \tag{46}$$

$$\Gamma_3 = \frac{K' \sigma_\phi^2 \lambda^2}{\bar{D} + 2\beta g} \left( \bar{C}_{\mu 0} + D' \frac{\partial^2 \bar{C}}{\partial x^2} \right) \tag{47}$$

where $D' = d\bar{D}/d\bar{\phi} > 0$ and $K' = d\bar{K}/d\bar{\phi} < 0$ in agreement with our discussion in Sect. 2.1.

Based on the analytical part of our investigation, the following fundamental observations on the structure of the upscaled differential equations can be made:

1. Upscaling introduces clearly defined new terms into the governing equations. These are the diffusive term, involving apparent diffusivity, $\mathcal{D}$, and the source/sink terms: $\Gamma_1$, $\Gamma_2$, and $\Gamma_3$ in Eq. 43.
2. In the homogeneous limit, the parameters $\sigma_\phi^2$ and $\lambda$ are nil; hence, the apparent diffusion coefficient, $\mathcal{D}$, reduces to $\bar{D}$, and $\Gamma_i$ terms all disappear. Thus, Eq. 43 become identical with the Eq. (11), i.e., the homogeneous case.
3. $\mathcal{D}$ is influenced by the presence of viscous transport, and its physical interpretation appears complex.
4. $\Gamma_i$ increase with the variance of porosity, $\sigma_\phi^2$.
5. $\Gamma_2$ and $\Gamma_3$ show dependence on the free gas concentration, and therefore they are expected to change in time and space.
6. $\Gamma_1$ and $\Gamma_3$ increase with the initially available mean adsorbed gas amount, $\bar{C}_{\mu 0}$

In the following section, the obtained upscaled governing equations given in (43) are numerically analyzed using a time-implicit finite difference approach based on Newton method and using gas/matrix system parameters given in Table 1, and considering the initial/boundary value problem defined in Fig. 5. The data set includes the local (or laboratory measured) viscous and diffusive transport, and kinetics parameters for a symmetric matrix block (slab) with a half-length of 10.0 cm and surrounded by fracture; in addition, it introduces a mildly heterogeneous matrix as base-case for the sensitivity analysis. At a particular time-step during the simulation, as part of the Newton iteration, the mean-field approximation of the free gas concentration $g$ and its derivative with respect to porosity, $g'$, are computed. Results are presented in terms of the free and adsorbed gas concentration profiles, and fractional recovery curves in the Figs. 6–9.

## 5 Results and Discussion

Our analysis involves two types of numerically obtained data, which correspond to a matrix considered to be (i) homogeneous, or (ii) heterogeneous. In the latter case, the analysis

**Table 1** Problem parameters for the heterogeneous gas–matrix system

| Parameter | Unit | Value |
|---|---|---|
| $\bar{\phi}$ | fraction | 1.0E−2 |
| $\sigma_{\phi}^2$ | – | 5.3E−7 |
| $\bar{C}_0$ | mol/cc | 2.0E−3 |
| $k_{\mathrm{r}}$ | 1/s | 1.0E−5 |
| $\bar{K}$ | fraction | 0.1 |
| $g$ | mol/cc | 2.028E−4 |
| $B_0$ | $\mathrm{cm}^2$ | 4.934E−14 |
| $\mu_g$ | kg/cm s | 2.0E−7 |
| $K'$ | fraction | −5.0E2 |
| $\bar{D}$ | $\mathrm{cm}^2$/s | 1.0E−3 |
| $D'$ | $\mathrm{cm}^2$/s | 3.3E−2 |
| $g'$ | mol/cc | −0.00835 |
| $\hat{\alpha}$ | cm/s | 6.0E−9 |
| $\lambda$ | cm | 1.0 |
| $L$ | cm | 10.0 |
| $T$ | Kelvin | 293.15 |

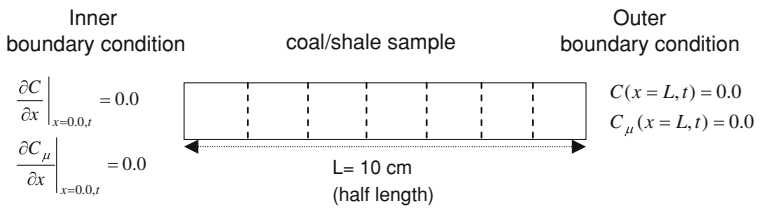


**Fig. 5** A schematic showing the setup for numerical simulation. $\delta x_i = 10/500\,\mathrm{cm}$ and $\delta t_i = 1.4\,\mathrm{min}$ for $i = 1, 2, \ldots, 500$, $C(x, t = 0) = 2.0\mathrm{E}{-3}$, $C_\mu(x, t = 0) = 2.0\mathrm{E}{-4}\,\mathrm{mol/cc}$

requires that the simulations are run under varying conditions of heterogeneity. Heterogeneous matrix properties with the base-state values are also given in Table 1.

Figure 6 shows the direct comparison of the heterogeneous case with the equivalent homogeneous case, in terms of free/adsorbed gas concentration profiles and fractional gas recovery curve. It is observed that heterogeneity retards gas release from the matrix and influences gas recovery adversely. The ultimate recovery, which was 100% in the homogeneous case, drops to a value around 87.0% in the mildly heterogeneous case. Understanding how the matrix heterogeneity influences the gas behavior, as depicted in Fig. 6, requires several steps of analysis. For this purpose, first, a sensitivity analysis is performed through numerical simulation and comparing the magnitudes of the terms appearing in (43).

Based on the sensitivity analysis, it is found that $\mathcal{D} \cong \bar{D}$; hence, mild fluctuations in porosity has negligible effect on molecular diffusion in porous media. In addition, it is found that $\Gamma_2$ is negligible for the typical coalbed and gas shale conditions, and $\Gamma_3$ safely reduces to the following form:

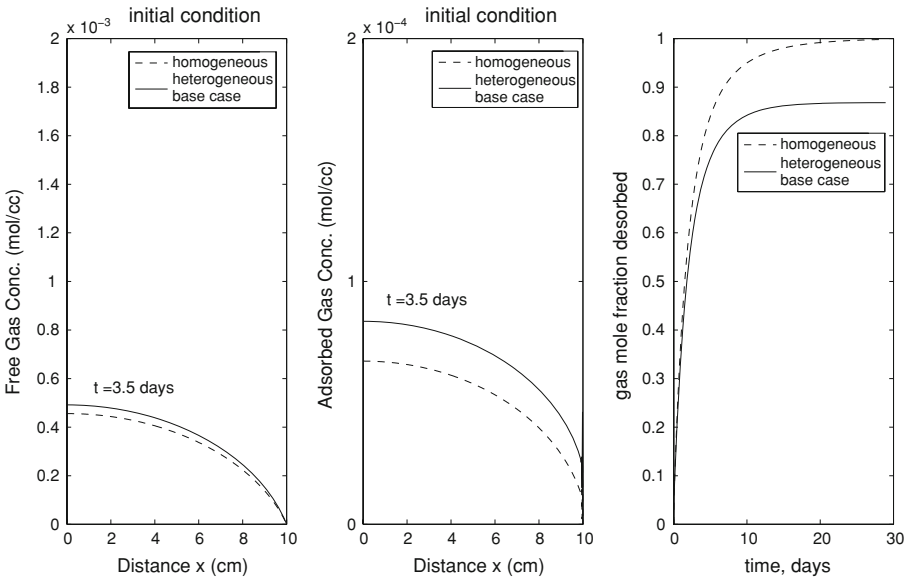


**Fig. 6** Effect of porosity heterogeneity on gas recovery. *Left* Free gas concentration profile versus distance from the center of matrix. *Middle* Adsorbed gas concentration profile versus distance from the center of the matrix. *Right* Gas mole fraction desorbed versus time

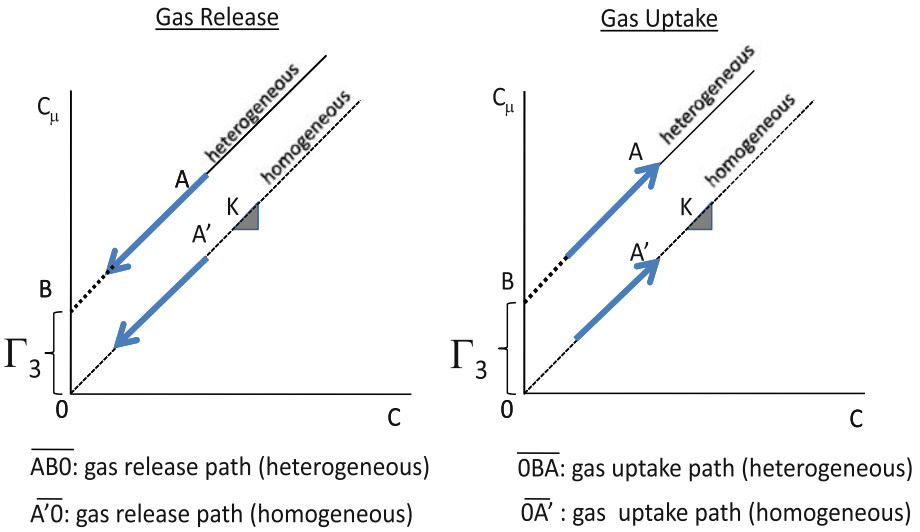


**Fig. 7** Effect of $\Gamma_3$ on gas release (*left*) and gas uptake (*right*) under the equilibrium adsorption condition

$$\Gamma_3 \cong \frac{K'\lambda^2\sigma_\phi^2\bar{C}_{\mu 0}}{\bar{D}+2\beta g} \tag{48}$$

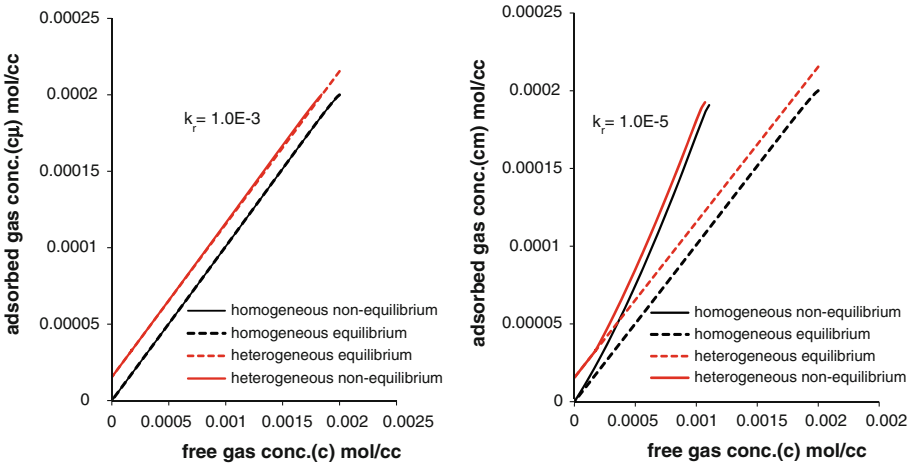


**Fig. 8** Effect of sorption on gas behavior in homogeneous and heterogeneous porous media. Free gas versus adsorbed gas concentrations at the center of the matrix block

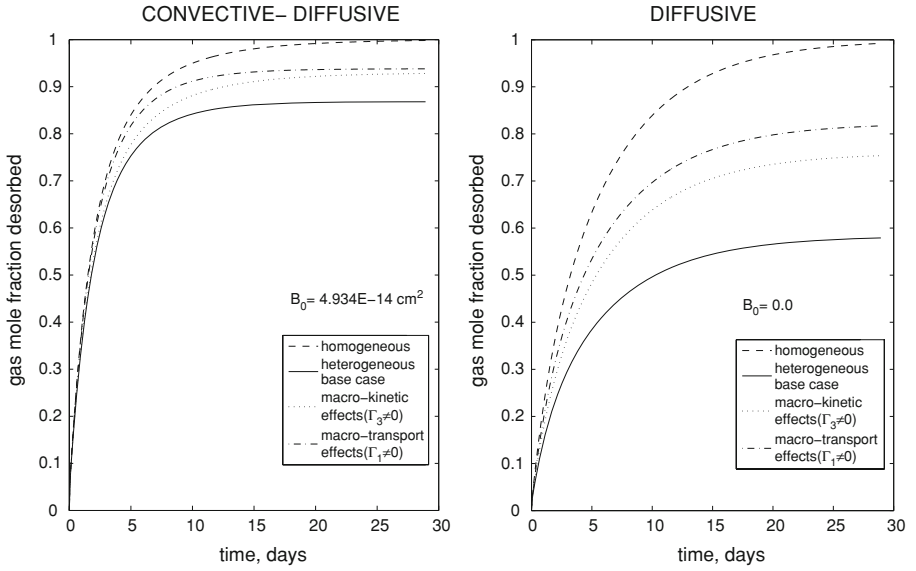


**Fig. 9** Macro-kinetics and macro-transport effects on the ultimate gas recovery. Fractional gas recovery versus time for a convective–diffusive (*left*) and for a diffusive (*right*) system with zero permeability

## 5.1 Macro-Transport Effect

Further, it is observed that typically $\bar{\phi} g' \ll g$ condition is satisfied across the matrix block; hence, $\Gamma_1$ simplifies to

$$\Gamma_1 \cong \left( \frac{\bar{D}}{\bar{D} + 2\beta g} + \frac{\beta g}{\bar{D} + 2\beta g} \right) \sigma_\phi^2 \bar{C}_{\mu 0}. \tag{49}$$

Substituting the definitions of $\beta$ and $g$ into this approximation and re-arranging, the following expression is obtained:

$$\Gamma_1 \cong \left[\frac{1}{1+\dfrac{2B_0\bar{\bar{p}}}{\bar{D}\mu}}+\frac{1}{2+\dfrac{\bar{D}\mu}{B_0\bar{\bar{p}}}}\right]\sigma_\phi^2\bar{C}_{\mu 0}=\frac{\sigma_\phi^2\bar{C}_{\mu 0}}{1+N_{Pe}/(1+N_{Pe})}. \tag{50}$$

Here, $\bar{\bar{p}}=RT\bar{\bar{C}}$ is the average pressure across the matrix and the denominator includes a dimensionless quantity, $N_{Pe}$, commonly known as Péclet number. It is a measure of the rate of viscous transport of a flow to its rate of molecular diffusion. Hence, for typical coal and shale matrices, $\Gamma_1$ increases with the matrix permeability. However, note that it does not disappear in the zero permeability limit; instead, it changes with the average initial adsorbed gas amount and with the porosity variance (This limit will be further discussed in Sect. 5.3). Thus, $\Gamma_1$ is truly a term corresponding to macro-transport effect of the heterogeneous matrix.

### 5.2 Macro-Kinetics Effect

Similarly, one can re-visit the expression of $\Gamma_3$ by substituting the definitions of $\beta$ and $g$ into the approximation:

$$\Gamma_3 \cong \frac{K'\sigma_\phi^2\lambda^2\bar{C}_{\mu 0}}{\bar{D}+\dfrac{2B_0\bar{\bar{p}}}{\mu}}=\frac{K'\lambda^2}{\bar{D}\left(1+\dfrac{2B_0\bar{\bar{p}}}{\bar{D}\mu}\right)}\sigma_\phi^2\bar{C}_{\mu 0}=\frac{N_{Th}}{k_r(1+2N_{Pe})}\sigma_\phi^2\bar{C}_{\mu 0}, \tag{51}$$

which now includes a modified Thiele modulus, $N_{Th}=(\mathrm{d}\bar{K}/\mathrm{d}\bar{\phi})k_r\lambda^2/\bar{D}$ for the heterogeneous matrix. In our case, Thiele modulus is a measure of the porosity dependence of the adsorption rate with respect to the rate of diffusion and, interestingly, its definition now includes the correlation length of the heterogeneous porosity field. As in the case of macro-transport term, $\Gamma_3$ increases with the average initial adsorbed gas amount and with the porosity variance. Hence, $\Gamma_3$ reflects macro-kinetics effect of the heterogeneous matrix.

One can have a more insightful look at the macro-kinetics effect in the equilibrium adsorption limit. Note that under the equilibrium conditions, we now have

$$\bar{K}\bar{C}-\left(\bar{C}_\mu+\Gamma_3\right)=0, \tag{52}$$

which gives

$$\bar{C}_\mu=\bar{K}\bar{C}-\Gamma_3 \tag{53}$$

when re-organized. A schematic representation of the macro-kinetics effect is shown in Fig. 7 for both gas uptake and release cases. For a given free gas amount, the macro-kinetics effect (or $\Gamma_3$) causes the matrix to retain a larger amount of adsorbed gas, which creates trapping effect during the gas release and a threshold effect during the gas uptake. These observations are confirmed using numerical results, which are shown in Fig. 8.

Figure 9 (left) delineates the macro-transport and macro-kinetics effects of heterogeneity, i.e., it investigates the influences of $\Gamma_1$ and $\Gamma_3$ on the fractional gas recovery curve separately. Obviously, macro-transport and -kinetics both play an active role on the reduction in gas recovery observed earlier, see Fig. 6 (right).

### 5.3 Diffusive limit: $N_{Pe} \to 0$

When permeability is low, typically in the order of nano-darcy, the convective transport term in our upscaled free gas mass balance vanishes. In this limit, Eqs. 50 and 51 reduce to

$$\begin{aligned} \Gamma_{1,\text{diff}} &= \sigma_\phi^2 \bar{C}_{\mu 0} \\ \Gamma_{3,\text{diff}} &= \tfrac{N_{Th}}{k_\text{r}} \sigma_\phi^2 \bar{C}_{\mu 0} \end{aligned} \tag{54}$$

Substituting equation (54) into the upscaled equation (43), and considering $\mathcal{D}$ and $\Gamma_2$ as negligible, the upscaled equation for diffusive system becomes:

$$\begin{aligned} \bar{\phi} \frac{\partial \bar{C}}{\partial t} + (1-\bar{\phi}) \frac{\partial \bar{C}_\mu}{\partial t} &= \frac{\partial}{\partial x} \left( \bar{\phi} \bar{D} \frac{\partial \bar{C}}{\partial x} \right) + \sigma_\phi^2 \bar{C}_{\mu 0} \\ \frac{\partial \bar{C}_\mu}{\partial t} &= k_\text{f} \bar{C} - k_\text{r} \bar{C}_\mu + N_{Th} \sigma_\phi^2 \bar{C}_{\mu 0} \end{aligned} \tag{55}$$

Figure 9 (right) shows the diffusive system response in terms of gas recovery. We note that the absence of viscous transport does not influence the homogeneous response significantly because, during the same time period, almost the same amount of gas is ultimately recovered using diffusion as the only transport mechanism; see slightly lower dashed line on Fig. 9 (right) and compare with the other dashed line on Fig. 9 (left). Intuitively, one would expect such behavior in the case of coal and shale matrices because these environments maintain relatively low permeability. Interestingly, however, the same argument may not be raised when the matrix is considered to be heterogenous (see the solid lines in Fig. 9). Less than 60% of the gas initially in-place could be recovered during the same time period when the gas transport is due to diffusion only. This reduction is due to macro-transport and, more importantly, to the macro-kinetics effects of the porosity heterogeneity, as they persist in the diffusive limit. Furthermore, depending on Thiele modulus, the macro-kinetics effect has the potential to dominate the ultimate gas recovery.

## 6 Conclusion

In this article, the gas flow, diffusive transport, and adsorption in heterogeneous porous media resembling coal and shale matrices are investigated using a theoretical approach. In addition, unlike previous theoretical works, the sorption rates are explicitly introduced to a mathematical framework in this context.

Random local variations in matrix pore structure and material content are considered, and their influence on gas sorption and transport are investigated using small perturbations theory, a proven technique widely used in various other disciplines where analysis of multi-physics problems are required in the presence of a priori fluctuations induced by non-uniform fields. In conclusion, the homogenized gas–matrix system behavior can be described using the following upscaled governing equations

$$\begin{aligned} \phi \frac{\partial C}{\partial t} + (1-\phi) \frac{\partial C_\mu}{\partial t} &= \frac{\partial}{\partial x} \left( \phi D \frac{\partial C}{\partial x} \right) + \frac{\partial}{\partial x} \left( \phi C \frac{B_0}{\mu} \frac{\partial p}{\partial x} \right) + \frac{\sigma_\phi^2 \bar{C}_{\mu 0}}{1 + N_{Pe}/(1+N_{Pe})} \\ \frac{\partial C_\mu}{\partial t} &= k_\text{f} C - k_\text{r} C_\mu + \frac{N_{Th}}{1 + 2N_{Pe}} \sigma_\phi^2 \bar{C}_{\mu 0} \end{aligned} \tag{56}$$

Further, it is found that the matrix heterogeneity generates non-trivial, macro-transport, and macro-kinetics effects on the system. The system behavior is investigated numerically

and it is found that macro-kinetics and macro transport have the potential to reduce the ultimate gas recoveries significantly.

**Acknowledgments** The authors gratefully acknowledge the support received from the University of Oklahoma, Mewbourne School of Petroleum and Geological Engineering, MPGE, and from the Natural Science and Engineering Research Council of Canada, NSERC, for the completion of this study.

## Appendix A

See Tables 2 and 3.

**Table 2**

$$P_{ks} = \sum_{m=1,2} \int \frac{1}{2\pi} G^{-1}_{k-Q\,s} \overline{\xi_{Qm} \tilde{\Phi}_{-Q}}\, [i(k-Q)]^m \, \mathrm{d}Q$$

$$Q_{ks} = \sum_{m,n=1,2} \int \frac{1}{2\pi} G^{-1}_{k-Q\,s} \overline{\xi_{Qm} \xi_{-Qn}}\, [i(k-Q)]^m \, (ik)^n \mathrm{d}Q$$

$$S_{ks} = \sum_{m=1,2} \int \frac{1}{2\pi} G^{-1}_{k-Q\,s} \beta \overline{\xi_{Qm} \tilde{\alpha}'_{-Q}}\, [i(k-Q)]^m \, (ik) \mathrm{d}Q$$

$$T_{ks} = \sum_{m=1,2} \int \frac{1}{2\pi} L_{k-Q\,s} \overline{\xi_{Qm} \tilde{K}_{-Q}}\, [i(k-Q)]^m \, \mathrm{d}Q$$

$$U_{ks} = \int \frac{1}{2\pi} G^{-1}_{k-Q\,s} \beta \overline{\tilde{\alpha}'_{Q} \tilde{\Phi}_{-Q}}\, [i(k-Q)] \, \mathrm{d}Q$$

$$V_{ks} = \sum_{m=1,2} \int \frac{1}{2\pi} G^{-1}_{k-Q\,s} \beta \overline{\xi_{Qm} \tilde{\alpha}'_{-Q}}\, [i(k-Q)] \, (ik)^m \mathrm{d}Q$$

$$W_{ks} = \int \frac{1}{2\pi} G^{-1}_{k-Q\,s} \beta^2 \overline{\tilde{\alpha}'_{Q} \tilde{\alpha}'_{Q}}\, [i(k-Q)] \, (ik) \mathrm{d}Q$$

$$Y_{ks} = \int \frac{1}{2\pi} L_{k-Q\,s} \overline{\tilde{\alpha}'_{Q} \tilde{K}_{-Q}}\, [i(k-Q)] \, \mathrm{d}Q$$

$$Z_{ks} = \int \frac{1}{2\pi} \breve{G}^{-1}_{k-Q\,t=0} \overline{\tilde{\Phi}_{Q} \tilde{\Phi}_{-Q}} \mathrm{d}Q$$

$$M_{ks} = \sum_{m=1,2} \int \frac{1}{2\pi} \breve{G}^{-1}_{k-Q\,t=0} \overline{\tilde{\Phi}_{Q} \xi_{Qm}} (ik)^m \mathrm{d}Q$$

$$N_{ks} = \int \frac{1}{2\pi} \breve{G}^{-1}_{k-Q\,t=0} \beta \overline{\tilde{\alpha}'_{Q} \tilde{\Phi}_{-Q}} (ik) \mathrm{d}Q$$

$$O_{ks} = \int \frac{1}{2\pi} \breve{L}_{k-Q\,t=0} \overline{\tilde{K}_{Q} \tilde{\Phi}_{-Q}} \mathrm{d}Q$$

**Table 3**

$$I_{ks} = \int \frac{1}{2\pi} G^{-1}_{k-Q\,s} \overline{\tilde{K}_{Q} \tilde{\Phi}_{-Q}} \mathrm{d}Q$$

$$E_{ks} = \int \frac{1}{2\pi} G^{-1}_{k-Q\,s} \overline{\tilde{K}_{Q} \tilde{\alpha}_{-Q}}\, ik \mathrm{d}Q$$

$$F_{ks} = \int \frac{1}{2\pi} G^{-1}_{k-Q\,s} \overline{\tilde{K}_{Q} \tilde{D}_{-Q}}\, (ik)^2 \mathrm{d}Q$$

$$J_{ks} = \int \frac{1}{2\pi} L_{k-Q\,s} \overline{\tilde{K}_{Q} \tilde{K}_{-Q}}\, \mathrm{d}Q$$

## Appendix B

See Table 4.

**Table 4**

$$\overline{\tilde{\Phi}_{-Q}\tilde{\alpha}_{Q}} = i\left(D' + \bar{D}/\bar{\phi}\right)\sigma_{\phi}^{2} Q\sqrt{2\pi}\lambda \exp\left(-Q^{2}\lambda^{2}/2\right)$$

$$\overline{\tilde{\Phi}_{-Q}\tilde{D}_{Q}} = D'\sigma_{\phi}^{2}\sqrt{2\pi}\lambda \exp\left(-Q^{2}\lambda^{2}/2\right)$$

$$\overline{\tilde{\alpha}_{Q}\tilde{\alpha}_{-Q}} = \left(D' + \bar{D}/\bar{\phi}\right)^{2}\sigma_{\phi}^{2} Q^{2}\sqrt{2\pi}\lambda \exp\left(-Q^{2}\lambda^{2}/2\right)$$

$$\overline{\tilde{D}_{-Q}\tilde{\alpha}_{Q}} = \overline{\tilde{\alpha}_{Q}\tilde{D}_{-Q}} = iD'\left(D' + \bar{D}/\bar{\phi}\right)\sigma_{\phi}^{2} Q\sqrt{2\pi}\lambda \exp\left(-Q^{2}\lambda^{2}/2\right)$$

$$\overline{\tilde{D}_{-Q}\tilde{D}_{Q}} = D'^{2}\sigma_{\phi}^{2}\sqrt{2\pi}\lambda \exp\left(-Q^{2}\lambda^{2}/2\right)$$

$$\overline{\tilde{\Phi}_{-Q}\tilde{\alpha}'_{Q}} = i\left(C' + \bar{C}/\bar{\phi}\right)\sigma_{\phi}^{2} Q\sqrt{2\pi}\lambda \exp\left(-Q^{2}\lambda^{2}/2\right)$$

$$\overline{\tilde{\Phi}_{-Q}\tilde{\Phi}_{Q}} = \sigma_{\phi}^{2}\sqrt{2\pi}\lambda \exp\left(-Q^{2}\lambda^{2}/2\right)$$

$$\overline{\tilde{\Phi}_{-Q}\tilde{K}_{Q}} = K'\sigma_{\phi}^{2}\sqrt{2\pi}\lambda \exp\left(-Q^{2}\lambda^{2}/2\right)$$

$$\overline{\tilde{K}_{-Q}\tilde{\alpha}'_{Q}} = iK'\left(C' + \bar{C}/\bar{\phi}\right)\sigma_{\phi}^{2} Q\sqrt{2\pi}\lambda \exp\left(-Q^{2}\lambda^{2}/2\right)$$

$$\overline{\tilde{\alpha}'_{Q}\tilde{\alpha}'_{-Q}} = \left(C' + \bar{C}/\bar{\phi}\right)^{2}\sigma_{\phi}^{2} Q^{2}\sqrt{2\pi}\lambda \exp\left(-Q^{2}\lambda^{2}/2\right)$$

$$\overline{\tilde{\alpha}_{Q}\tilde{\alpha}'_{-Q}} = \left(C' + \bar{C}/\bar{\phi}\right)\left(D' + \bar{D}/\bar{\phi}\right)\sigma_{\phi}^{2} Q^{2}\sqrt{2\pi}\lambda \exp\left(-Q^{2}\lambda^{2}/2\right)$$

$$\overline{\tilde{D}_{Q}\tilde{\alpha}'_{-Q}} = iD'\left(C' + \bar{C}/\bar{\phi}\right)\sigma_{\phi}^{2} Q\sqrt{2\pi}\lambda \exp\left(-Q^{2}\lambda^{2}/2\right)$$

$$\overline{\tilde{K}_{-Q}\tilde{\alpha}_{Q}} = iK'\left(D' + \bar{D}/\bar{\phi}\right)\sigma_{\phi}^{2} Q\sqrt{2\pi}\lambda \exp\left(-Q^{2}\lambda^{2}/2\right)$$

$$\overline{\tilde{K}_{-Q}\tilde{D}_{Q}} = K'D'\sigma_{\phi}^{2}\sqrt{2\pi}\lambda \exp\left(-Q^{2}\lambda^{2}/2\right)$$

## References


Alvarado, V., Scriven, L.E., Davis, H.T.: Stochastic-perturbation analysis of a one-dimensional dispersion-reaction equation: effects of spatially-varying reaction rates. Transp Porous Media **32**, 139–161 (1998)

Brusseau, M.L., Jessup, R.E., Rao, P.S.C.: Nonequilibrium sorption of organic chemicals: elucidation of rate limiting processes. Environ. Sci. Technol. **25**, 134–142 (1991)

Do, D.D., Wang, K.: A new model for the description of adsorption kinetics in heterogeneous activated carbon. Carbon **36**(10), 1539–1554 (1998)

Dubinin, M.M.: Chemistry and Physics of Carbon. Marcel Dekker, New York (1966)

Forster, D.: Hydrodynamics Fluctuations, Broken Symmetry and Correlation Functions. Benjamin-Cummings, Reading, MA (1977)

Gelhar, L.W.: Stochastic Subsurface Hydrology. Prentice Hall, Englewood Cliffs (1993)

Hu, B.X., Deng, F., Cushman, J.H.: Non-local reactive transport with physical and chemical heterogeneity: linear non-equilibrium sorption with random $K_d$. Water Resour. Res. **31**(9), 2239–2252 (1995)

Jagiello, J., Bandosz, T.J., Putyera, K., Schwarz, J.A.: Micropore structure of template-derived carbons studied using adsorption of gases with different molecular diameters. J. Chem. Soc., Faraday Trans. **91**, 2929–2933 (1995)

Jenkins, C.D., Boyer, C.M., II: Coalbed- and shale-gas reservoirs. J. Petrol. Technol. **60**(2), 92–99 (2008)

Karacan, O.C.: An effective method for resolving spatial distribution of adsorption kinetics in heterogeneous porous media: applied for carbon dioxide sequestration in coal. Chem Eng. Sci. **58**, 4681–4693 (2003)

King, G.R.: Material balance techniques for coal seam and Devonian Shale. SPE 20730 (1990)

L'Heureux, I.: Stochastic reaction-diffusion phenomena in porous media with nonlinear kinetics: effects of quenched porosity fluctuations. Phys. Rev. Lett. **93**(18), 180602 (2004)

Nuttall, B.C.: Analysis of Devonian black shales in Kentucky for potential carbon dioxide sequestration and enhanced natural gas production. Kentucky Geological Survey Report DE-FC26-02NT41442 (2005)

Ruckenstein, E., Vaidyanathan, A.S., Youngquist, G.R.: Sorption by solids with bidisperse pore structures. Chem. Eng. Sci. **26**, 1305–1318 (1971)

Smith D.M., Williams F.L.: Diffusional effects in the recovery of methane from coalbeds. Soc. Petrol. Eng. J. **24**, 529–535 (1984)

Weida S.D., Lambert S.W., Boyer II, C.M.: Challenging the traditional coalbed methane exploration and evaluation. SPE 98069 (2005)